D. Haigh and J. A. Pyle, *Q. J. R. Meteorol. Soc.* **108**, 551 (1982); F. Stordal and I. S. A. Isaksen, *Tellus* **39B**, 333 (1987); H. S. Johnston *et al.*, *Atmospheric Ozone 1985* (World Meteorological Organization, Geneva, 1966), chap. 13.
4. S. Solomon *et al.*, *J. Geophys. Res.* **90**, 12981 (1985).
5. J. D. Haigh, *Q. J. R. Meteorol. Soc.* **110**, 167 (1984).
6. R. S. Eckman, J. D. Haigh, J. A. Pyle, *Nature (London)* **329**, 616 (1987). This study is based on a classical Eulerian 2-D model that includes most of the important feedbacks between chemistry and radiation but uses satellite data to specify momentum and heat fluxes associated with large-scale waves.
7. J. J. Barnett, J. T. Houghton, J. A. Pyle, *Q. J. R. Meteorol. Soc.* **101**, 245 (1975); G. M. Keating, G. P. Brasseur, J. Y. Nicholson III, A. De Rudder, *Geophys. Res. Lett.* **12**, 449 (1985).
8. H. J. Edmon Jr., B. J. Hoskins, M. E. McIntyre, *J. Atmos. Sci.* **37**, 2600 (1980); T. J. Dunkerton, C. P. F. Hsu, M. E. McIntyre, *ibid.* **38**, 819 (1981).
9. R. S. Lindzen, *J. Geophys. Res.* **86**, 9707 (1981); G. Brasseur and M. Hitchman, in *Proceedings of the NATO Workshop on Middle Atmosphere Transport* (Reidel, Dordrecht, 1987).
10. M. H. Hitchman and G. Brasseur, unpublished results. Mixing and the meridional circulation caused by Rossby waves are parameterized in the 2-D model by using the conservation of wave activity principle. Rossby wave activity is produced in a climatological fashion at the tropopause, advected by a group velocity that evolves with the model zonal winds, and is damped at upper levels. Absorption of Rossby wave activity causes both an easterly torque and irreversible mixing. This parameterization provides a self-consistent coupling of the wave activity with the winds, tracer distributions, and the radiative field.
11. D. L. Williamson, J. T. Kiehl, V. Ramanathan, R. E. Dickinson, J. J. Hack, *NCAR Tech. Note 285* (National Center for Atmosphere Research, Boulder, CO, 1987).
12. G. Brasseur and S. Solomon, *Aeronomy of the Middle Atmosphere* (Reidel, Dordrecht, 1987).
13. W. B. De More *et al.*, *JPL Publ. 85–97* (National Aeronautics and Space Administration/Jet Propulsion Laboratory, Washington, DC, 1985); G. Brasseur and P. C. Simon, *J. Geophys. Res.* **86**, 7343 (1981).
14. M. C. McCracken and F. M. Luther, *U.S. Dep. Energy DOE/ER-0237* (1985).
15. C. B. Leovy, in *Dynamics of the Middle Atmosphere* (Terra Scientific, Tokyo, 1984).
16. The National Center for Atmospheric Research is sponsored by the National Science Foundation. We thank J. T. Kiehl for providing the radiative code and J. C. Gille and B. A. Boville for useful discussions.

6 November 1987; accepted 19 February 1988

Iron Photoreduction and Oxidation in an Acidic Mountain Stream

D. M. McKnight, B. A. Kimball, K. E. Bencala

In a small mountain stream in Colorado that receives acidic mine drainage, photoreduction of ferric iron results in a well-defined increase in dissolved ferrous iron during the day. To quantify this process, an instream injection of a conservative tracer was used to measure discharge at the time that each sample was collected. Daytime production of ferrous iron by photoreduction was almost four times as great as nighttime oxidation of ferrous iron. The photoreduction process probably involves dissolved or colloidal ferric iron species and limited interaction with organic species because concentrations of organic carbon are low in this stream.

Hydrous iron oxides, which commonly occur in aquatic environments, may influence the chemistry and transport of trace metals and natural organic material by adsorption and coprecipitation reactions. We present results of a field experiment in which production of ferrous iron, Fe(II), by photoreduction was measured quantitatively in a small Rocky Mountain stream that receives acidic mine drainage. A well-defined increase in dissolved Fe(II) occurred with increasing light intensity. There are several pathways by which diel cycling of iron through photoreduction and oxidation will influence other chemical or microbial processes. This diel cycle may contribute to the increased abundance of amorphous iron oxides over that of more crystalline forms in streams; amorphous oxides are more reactive in adsorbing metal and organic species (*1*). Diel photoreduction and oxidation of iron, and other metals such as copper (*2*), may be a source of scatter in long-term data sets of metal concentrations in acidic streams and lakes (*3*).

St. Kevin Gulch, in Colorado, is representative of the more than 600 km of stream reach in the state that is contaminated with acidic mine drainage (*4*). This small tributary of Tennessee Creek is located 7 km northwest of Leadville and receives acidic, metal-enriched drainage (*5*) from mine tailings and abandoned mines (Fig. 1). Silver sulfide ore in veins in quartz-biotite-feldspar schist and gneiss was mined more than 80 years ago. The 247-m reach that was studied (between sites SK40 and SK50 in Fig. 1) begins 1185 m downstream from the inflows from the tailings. Hydrous iron oxides are abundant on the stream bed in the study area.

Accurate measurement of discharge is necessary for calculation of mass flow (*6*). We used the dilution gauging technique (*7, 8*); a solution of 4.8*M* LiCl was injected into the stream at a site 360 m above the mine at a constant rate of 27 ml min^{-1} during a 36-hour period. The steady-state Li^+ concentration was 0.76 ± 0.02 mg $liter^{-1}$ at SK40 and 0.75 ± 0.02 mg $liter^{-1}$ at SK50 (mean ± SEM, n = 40). Background Li^+ concentrations were approximately 0.004 mg $liter^{-1}$. Discharge was calculated from the mass balance of the injected Li^+ and the concentration of Li^+ in the stream for each time point at both sites. The travel time was about 4 hours from the mine site to SK40 and was 40 minutes from SK40 to SK50, as determined by comparing the leading and trailing edges of the injected tracers (*7, 8*).

Samples were collected at hourly intervals at SK40 and SK50 from before sunrise at 0500 on 19 August 1986 until 1800 on 20 August 1986 (*9, 10*). The iron concentrations that were determined by inductively coupled plasma spectrophotometry (ICP) for the 0.1-μm filtered samples (filterable iron) were consistently greater than iron concentrations that were obtained with addition of the hydroxylamine reductant in the colorimetric procedure (reactive iron) (Table 1). Ultrafiltration measurements showed that colloidal iron was about 50% of the filterable iron; because this amount was more than the difference between filterable and reactive iron, reactive iron probably included some colloidal iron as well. We calculated the activity ratio Fe^{2+}/Fe^{3+} and thus *Eh* by estimating ferric iron, Fe(III), as the difference between reactive and ferrous iron as determined colorimetrically; the program WATEQF (*11*) was used to calculate iron speciation (*12*).

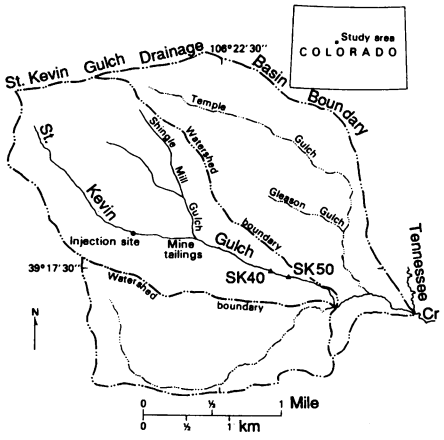

Fig. 1. Map of St. Kevin Gulch. The catchment area at SK50 is 3.9 km^2.

D. M. McKnight and B. A. Kimball, U.S. Geological Survey, Water Resources Division, Denver Federal Center, Denver, CO 80225.
K. E. Bencala, U.S. Geological Survey, Water Resources Division, 345 Middlefield Road, Menlo Park, CA 94025.

The photoreduction of Fe(III) species may be either a homogeneous reaction that involves dissolved species,

$$FeOH^{2+} \overset{h\nu}{\rightleftarrows} [Fe^{2+}\cdots(OH)] \rightarrow Fe^{2+} + \cdot OH \quad (1)$$

or a heterogeneous reaction such that a hydrous iron oxide solid phase absorbs near-ultraviolet radiation and releases Fe(II) to solution (*13–16*).

For the homogeneous reaction, the quantum yield of Fe(II) is about 10^{-2} mol $E_{250\text{–}425\ nm}^{-1}$, where $E_{250\text{–}425\ nm}$ is the radiant flux between 250 and 425 nm. Estimates of quantum yield are about 10^{-5} mol $E_{250\text{–}425nm}^{-1}$ for goethite, a common crystalline oxide, and amorphous hydrous Fe(III) oxides are more reactive (*14, 16*). Organic species may enhance the production of Fe(II) by scavenging hydroxyl radicals, which decreases the rate of reoxidation of Fe(II); furthermore, organic species that are adsorbed on hydrous Fe(III) oxides may assist in electron transfer through several mechanisms (*16*). However, the low concentration of organic carbon in St. Kevin Gulch (0.9 mg liter^{-1}), which is similar to that in other Rocky Mountain streams, indicates that high concentrations of organic species are not necessary to promote photoreduction.

At both sites and on both days, dissolved Fe(II) increased after sunrise (Fig. 2). Daytime Fe(II) concentrations were greater than nighttime values at both sites (Table 1). These results are best explained by photoreduction. In a study of an organic-rich stream, Madsen *et al.* showed that sunlight caused production of Fe(II) in both natural and poisoned streamwater-sediment mixtures, which indicates that biological processes are not responsible for light-induced Fe(II) production (*17*). Variations in the concentrations of other dissolved trace metals were either insignificant compared to analytical error or showed no significant diel trend (Table 1).

Greater variability in Fe(II) concentration during the day than at night (Fig. 2) also is indicative of photoreduction. The Fe(II) concentration at a given time and site depends in part on past exposure of the passing water parcel to near-ultraviolet (UV) radiation; therefore, transient changes in upstream exposure to sunlight that were caused by intermittent cloud cover in the afternoon may have caused the short-term changes in Fe(II) concentration. Small, short-term changes in *p*H (Fig. 2) could have also influenced Fe(II) concentration.

Concentrations of both filterable and reactive iron were greater at the upstream site (SK40) than at the downstream site (SK50) (Fig. 2). This trend indicates that colloidal oxides continued to aggregate and deposit along the stream reach and further supports the conclusion that reactive iron included colloidal hydrous iron oxides. Variations in the concentrations of filterable iron and reactive iron did not correlate with light intensity at either site (Fig. 2). These variations may have resulted from either actual diel changes in discharge or changes in the amount of precipitating hydrous iron oxide that was retained by the filter. Because a light-induced increase in filterable or reactive iron was not observed, absorption of near-UV radiation and photoreduction probably involved either dissolved Fe(III) species, mainly $Fe(OH)_2^+$, $FeOH^{2+}$, and Fe^{3+}, or colloidal hydrous iron oxides in the streamwater. In another study of an acidic mountain stream where Fe(II) was about 90% of the filterable (and reactive) iron, all forms of iron increased during the day, which indicates that photoreduction of hydrous iron oxides on the streambed released Fe(II) to the stream (*3*).

At SK40 the measured *E*h was lower during the day (about 0.58 V) than at night (about 0.63 V), and it followed the same pattern as *E*h values calculated from Fe^{3+}/Fe^{2+}. However, the timing of the transitions between low and high values did not coincide for calculated and measured *E*h. These data support the finding from a study

Table 1. Dissolved constituents in St. Kevin Gulch during 19 to 20 August 1986.

Constituent*	SK40† (mg liter^{-1})	SK50† (mg liter^{-1})
Sodium	2.4 ± 0.1	4.3 ± 0.24
Calcium	13.0 ± 0.3	2.7 ± 0.34
Magnesium	4.3 ± 0.2	13.0 ± 0.73
Strontium	0.03 ± 0.008	0.03 ± 0.007
Barium	0.02 ± 0.002	0.02 ± 0.002
Sulfate	90.7 ± 3.7	90.9 ± 4.13
Chloride	4.0 ± 0.3	4.0 ± 0.3
Silica	16.3 ± 0.3	16.3 ± 0.08
Total organic carbon	0.9	
Aluminum	2.0 ± 0.22	2.0 ± 0.22
Manganese	4.2 ± 0.1	4.2 ± 0.24
Zinc	8.6 ± 0.3	8.6 ± 0.5
Filterable iron	1.6 ± 0.1	1.4 ± 0.2
Reactive iron	1.1 ± 0.1	1.0 ± 0.1
Fe(II)-daytime	0.41 ± 0.19	0.46 ± 0.18
Fe(II)-nighttime	0.20 ± 0.03	0.18 ± 0.02
Lead	0.023 ± 0.056	0.01 ± 0.01
Copper	0.088 ± 0.003	0.088 ± 0.006
Cadmium	0.050 ± 0.004	0.051 ± 0.004
Nickel	0.013 ± 0.013	0.01 ± 0.008

*Filterable iron was analyzed by ICP; reactive iron and Fe(II) were analyzed colorimetrically. †Data from 40 water samples collected and filtered through 0.1-μm filters at hourly intervals at SK40 and SK50, average values and standard deviations are presented.

Table 2. Mass flow of Fe(II) in St. Kevin Gulch at selected times during 19 to 20 August 1986.

SK40			SK50		Change in mass flow (mmol sec^{-1})	Net photoreductive flux (10^{-4} mmol m^{-2} sec^{-1})
Time (hour)	PAR (μE m^{-2} sec^{-2})	Mass flow (mmol sec^{-1})	Time (hour)	Mass flow* (mmol sec^{-1})		
			19 August 1986			
0605	0.8	0.029	0645	0.047	0.018	0.47
0700	60	0.058	0740	0.090	0.032	0.82
0800	410		0840	0.134		
0900	1200	0.102	0940	0.189	0.085	2.21
1000	1500	0.140	1040	0.205	0.065	1.68
1100	590	0.178	1140	0.218	0.040	1.04
1200	IC†	0.178	1240	0.189	0.011	0.28
1300	IC	0.195	1340	0.215	0.020	0.52
2000	2.0	0.076	2040	0.066	−0.010	
2100	0.01	0.074	2140	0.059	−0.015	
2300	0	0.070	2340	0.061	−0.009	
2400	0	0.073	2440	0.068	−0.005	
			20 August 1986			
0100	0	0.070	0140	0.069	−0.001	
0200	0	0.070	0240	0.064	−0.006	
0300	0	0.093	0340	0.058	−0.035	
0400	0	0.069	0440	0.061	−0.008	
0500	0	0.070	0540	0.057	−0.013	
0600	0		0640	0.066		
0700	105	0.062	0740	0.074	0.014	0.36
0800	125	0.090	0840	0.104	0.014	0.36
0900	540	0.108	0940	0.119	0.011	0.28
1000	220	0.161	1040	0.143	−0.17	
1100	760	0.121	1140	0.184	0.063	1.63
1200	570	0.190	1240	0.262	0.072	1.86
1300	1250	0.185	1340	0.302	0.117	3.02

*Interpolated value. †Intermittant clouds.

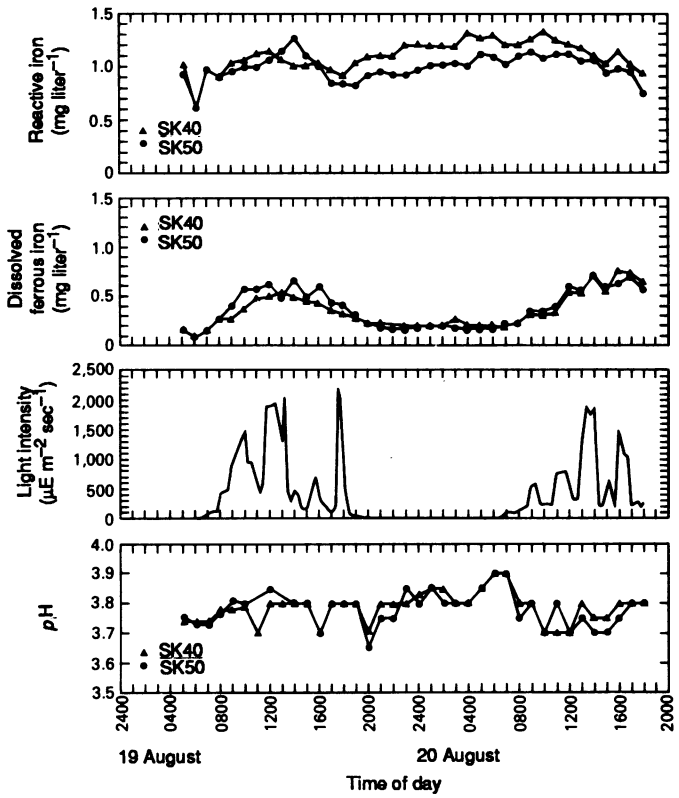

Fig. 2. Changes in reactive iron, ferrous iron, light intensity, and *p*H in St. Kevin Gulch on 19 and 20 August 1986.

on another stream with acidic mine drainage that the Fe(II)-Fe(III) couple controls measured *Eh* (*18*).

The mass flow (*6*) of Fe(II) (Table 2) was calculated from the measurements of discharge and Fe(II) concentration for each sample. The values at SK40 were compared with interpolated values at SK50 40 minutes after the sampling at SK40. The general trend is that during the day the Fe(II) mass flow is greater at the downstream site, whereas, during the night, the Fe(II) mass flow is smaller at the downstream site. The exception to this trend occurred at 1000 hours on the second day when light intensity decreased because of cloud cover. The increase in Fe(II) mass flow during the morning and midday ranged from 1.1×10^{-5} to 11.7×10^{-5} mol sec^{-1} with an average of $(4.3 \pm 0.9) \times 10^{-5}$ mol sec^{-1}. A net photoreductive flux (*6*) was calculated by dividing by the exposed free surface area of the stream (387 m^2), which yields an average value of 1.1×10^{-7} mol m^{-2} sec^{-1}.

Although net photoreductive flux was a cumulative measurement over 40 minutes and light intensity was, in contrast, an instantaneous measurement, a linear regression between these two parameters (values in Table 2) has a slope of $(1.4 \pm 0.3) \times 10^{-4}$ mol Fe(II) $E_{400-700nm}^{-1}$. This slope corresponds to an "effective quantum yield" of Fe(II) for the stream system of 1.4×10^{-3} mol $E_{250-425nm}^{-1}$, after correction for the proportion of near-UV radiation relative to photosynthetically active radiation (PAR) radiation (about 10%) (*9*, *19*). This estimate for effective quantum yield was determined on the basis of the radiation that is incident on the free surface of the stream. The true quantum yield would depend on the UV radiation that is actually absorbed by Fe(III) species in solution or colloidal iron oxides, and it would be corrected for oxidation rates and organic and inorganic complexation. Because the true quantum yield would be greater than the value obtained from the linear regression, the dominant reactions in this system may be solution phase reactions, which have quantum yields of 10^{-2} mol $E_{250-425nm}^{-1}$.

The Fe(II) concentration was fairly constant at night, which would be consistent with an upstream source of Fe(II) other than photoreduction. The Fe(II) mass flow consistently decreased between SK40 and SK50 at night; the average decrease for Fe(II) was $(1.1 \pm 0.3) \times 10^{-5}$ mol sec^{-1} (mean ± SEM, $n = 9$). This value is about a quarter of the average daytime net production of Fe(II) by photoreduction. This comparison shows that photoreduction is a critical process for enhancing iron transport and extending the downstream deposition of hydrous iron oxides.

If we assume that oxidation is a first-order rate process and do not consider the reduction of Fe(III), the oxidation rate of Fe(II) from SK40 to SK50 can be determined from the measured travel time, t, between the two sites (40 minutes) and

$$C_t = C_0 e^{-rt} \quad (2)$$

where C_0 is the concentration of Fe(II) at SK40, C_t is the interpolated concentration at SK50 40 minutes after the SK40 sample, and r is the rate constant. The calculated rate constant, 0.26 hour^{-1}, may be representative for the downstream reach bounded by SK40 and the confluence of St. Kevin Gulch with Tennessee Creek. The rate is comparable to those determined by Nordstrom (*18*), who measured oxidation rates that were five to six orders of magnitude greater than abiotic rates in another acidic mine drainage stream. The greater oxidation rate is probably a result of microbial processes (*18*).

If it is assumed that the Fe(II) oxidation rate that was measured at night is also representative of the oxidation rate during the day, an average gross production of Fe(II) by photoreduction can be calculated as the sum of the net daytime production (4.3×10^{-5} mol sec^{-1}) and the net nighttime loss (1.1×10^{-5} mol sec^{-1}). Gross production thus equals 5.5×10^{-5} mol sec^{-1}. Because oxidation is low compared to photoreductive production of Fe(II), rapid changes in iron speciation are possible in response to changes in solar radiation.

REFERENCES AND NOTES

1. D. K. Nordstrom, E. A. Jenne, J. W. Ball, in *Chemical Modeling in Aqueous Systems: Speciation, Sorption, Solubility and Kinetics*, E. A. Jenne, Ed. (Symposium Series 93, American Chemical Society, Washington, DC, 1979), pp. 51–79.
2. J. W. Moffet and R. G. Zika, in *Photochemistry of Environmental Aquatic System*, R. G. Zika and W. J. Cooper, Eds. (Symposium Series 327, American Chemical Society, Washington, DC, 1987), pp. 116–130.
3. D. M. McKnight and K. E. Bencala, in preparation.
4. R. E. Moran and D. A. Wentz, *Colo. Water Resour. Circ. 25* (1974).
5. B. A. Kimball, K. E. Bencala, D. M. McKnight, W. S. Maura, *U.S. Geol. Surv. Open-File Rep. 87-764*, in press.
6. Mass flow (moles per second) refers to transport in the downstream direction, net production (moles per second) refers to the increase in mass flow over a stream reach, and net photoreductive flux (moles per square meter per second) is net production per unit area of the free surface of the stream and corresponds to transport across a plane parallel to the free surface of the stream.
7. The basic methods of hydrologic tracer studies have been applied to acidic streams, and lithium has been shown to be a useful tracer (*8*).
8. V. C. Kennedy, *et al.*, *J. Hydrol.* 75, 67 (1984/1985); K. E. Bencala, D. M. McKnight, G. W. Zellweger, *Water Resour. Res.* 23, 827 (1987); K. E. Bencala, G. W. Zellweger, D. M. McKnight, *Eos* 68, 308 (1987).
9. Intensity of photosynthetically active radiation (PAR) (400 to 700 nm) was measured with a Li-cor LI-192SA underwater quantum sensor and LI-1000 data logger. We measured *p*H with a Beckman 21 meter and *Eh* with an Orion 399A ion analyzer immediately after collection. We used platinum electrodes for both measurements. Samples were then filtered through 0.1-μm Nuclepore filters with the use of an Antilla hand-held pump. Some samples were also filtered with a Millipore Pellicon OM-141

ultrafiltration unit with 100,000 molecular weight filter membranes. Metal samples were acidified with Ultrex HNO_3 (0.5 ml to 250 ml) and analyzed with model 975 Jarrel-Ash inductively coupled plasma (ICP) spectrophotometer. Lithium was also analyzed by flame atomic absorption spectrometry (Perkin-Elmer 2280 spectrophotometer). Anions were analyzed with a 2000i Dionex ion chromatograph. Organic carbon was measured with a Dohrmann carbon analyzer. Reagents for analysis of iron oxidation state by the 2,2'-bipyridine colorimetric method were added immediately after filtration to unacidified sample (*10*). Absorbance was measured within several hours for representative samples, and all samples were assayed within 2 days; the color development for the representative samples was stable over this period.

10. M. W. Skougstad *et al.*, *Techniques for Water Resources Investigations of the U.S. Geological Survey* (U.S. Geological Survey, Denver, 1986), Book 5, chapter A1, p. 387.
11. L. N. Plummer, B. F. Jones, A. H. Tresdell, *U.S. Geol. Surv. Water Res. Invest. 76-13* (1976).
12. J. I. Drever, *The Geochemistry of Natural Waters* (Prentice-Hall, Englewood Cliffs, NJ, 1982).
13. T. D. Waite and F. M. M. Morel, *J. Colloid Interface Sci.* **102**, 121 (1984).
14. ———, *Environ. Sci. Technol.* **18**, 860 (1984).
15. K. M. Cunningham, M. C. Goldberg, E. R. Weiner, *Photochem. Photobiol.* **41**, 409 (1985).
16. ———, in *Chemical Quality of Water and the Hydrologic Cycle*, R. A. Averett and D. M. McKnight, Eds. (Lewis Press, Ann Arbor, MI, 1987), p. 359.
17. E. L. Madsen, M. D. Morgan, R. E. Good, *Limnol. Oceanogr.* **31**, 832 (1986).
18. D. K. Norstrom, *U.S. Geol. Surv. Water-Supply Pap. 2270* (1985), pp. 113–119.
19. D. Dullin and T. Mill, *Environ. Sci. Technol.* **16**, 815 (1982).
20. Supported by the Hazardous Substances in Surface Waters Program of the U.S. Geological Survey–Water Resources Division. We acknowledge the sample collection efforts of D. H. Campbell, A. C. Duncan, R. M. Hirsch, C. L. Miller, B. D. Nordlund, B. Olver, R. C. Ruddy, N. E. Spahr, G. A. Wetherbee, and G. W. Zellweger, and comments on the manuscript by K. Nordstrom, D. Thorstenson, and D. Waite.

19 October 1987; accepted 10 March 1988

Toxic DNA Damage by Hydrogen Peroxide Through the Fenton Reaction in Vivo and in Vitro

JAMES A. IMLAY,* SHERMAN M. CHIN, STUART LINN†

Exposure of *Escherichia coli* to low concentrations of hydrogen peroxide results in DNA damage that causes mutagenesis and kills the bacteria, whereas higher concentrations of peroxide reduce the amount of such damage. Earlier studies indicated that the direct DNA oxidant is a derivative of hydrogen peroxide whose formation is dependent on cell metabolism. The generation of this oxidant depends on the availability of both reducing equivalents and an iron species, which together mediate a Fenton reaction in which ferrous iron reduces hydrogen peroxide to a reactive radical. An in vitro Fenton system was established that generates DNA strand breaks and inactivates bacteriophage and that also reproduces the suppression of DNA damage by high concentrations of peroxide. The direct DNA oxidant both in vivo and in this in vitro system exhibits reactivity unlike that of a free hydroxyl radical and may instead be a ferryl radical.

THE INSTABILITY OF PARTIALLY REduced oxygen species poses a serious threat to aerobic organisms. Consecutive univalent reductions of molecular oxygen to water produce three active intermediates, superoxide ($HO_2\cdot$), hydrogen peroxide (H_2O_2), and the hydroxyl radical ($HO\cdot$):

$$O_2 \xrightarrow[H^+]{e^-} HO_2\cdot \xrightarrow[H^+]{e^-} H_2O_2 \xrightarrow[H^+]{e^-} HO\cdot + H_2O \xrightarrow[H^+]{e^-} 2H_2O \quad (1)$$

Scavenging enzymes, such as catalase, peroxidase, and superoxide dismutase (*1*), and DNA repair enzymes that correct oxidative lesions (*2*) are found throughout the aerobic biota. Despite the apparent significance of oxidative cell damage, the mechanism and the ultimate oxidant have not yet been established.

At least two mechanisms produce cell damage in the killing of *Escherichia coli* by exogenous H_2O_2 (*3*). Starved cells can tolerate considerable exposure to H_2O_2 before they are killed; this "mode-two" killing is due to uncharacterized cell damage and exhibits a classical multiple-order dose-response curve. In "mode-one" killing, actively growing cells are killed by lower, more physiological doses of H_2O_2, particularly if they lack enzymes required for recombinational or base-excision DNA repair pathways.

In the mode-one response the rate of killing is maximal at ~2.5 m*M* H_2O_2 but is roughly independent of H_2O_2 concentration and half-maximal between about 10 and 20 m*M* (Fig. 1). (This twofold difference in rate gives rise to large differences in survival as shown in Fig. 2A.) Prior exposure to high doses of H_2O_2 does not increase resistance to an immediate subsequent challenge with low doses (*3*), indicating that this is not a protective response. Similar dose-response curves to H_2O_2 are obtained when monitoring mutagenesis, the extent of lysogenic phage lambda induction, or postdamage filamentation of surviving cells (*4*), each of which is thought to be related to the extent of DNA damage. (These latter effects as well as killing are eliminated at low H_2O_2 concentrations if cells are starved before challenge.) Thus the unusual nature of the dose response would appear to reflect a characteristic dose response for the generation of DNA damage.

Because mode-one killing and the related phenomena occur only in actively metabolizing cells, available reducing equivalents might be essential to convert H_2O_2 into a toxic oxidant. *E. coli* can be made to accumulate reducing equivalents if respiration is inhibited with cyanide; when so treated, normally resistant DNA repair-proficient cells become extremely sensitive to mode-one killing by H_2O_2 (Fig. 2A). Cyanide exerts this effect by blocking respiration, since *ndh* mutants, which lack active NADH dehydrogenase (where NADH is the reduced form of nicotinamide adenine dinucleotide) and are also nonrespiring, are highly sensitive to mode-one killing but are not made appreciably more so by the addition of cyanide (Fig. 2, B and C).

The $HO\cdot$ radical, a highly reactive oxidant, has been implicated in peroxide-mediated oxidation of a variety of substrates (*5*). The univalent reduction of H_2O_2 was postu-

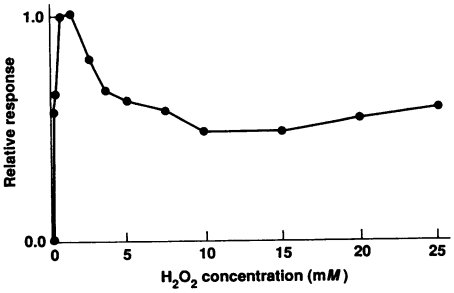

Fig. 1. Dependence of cellular responses on H_2O_2 concentration. The rate of killing of strain BW544 (*nfo xth*, defective in excision repair of oxidative DNA damage) is shown. Cells were exposed to H_2O_2 for 15 minutes and then plated. Colonies were counted after 24 to 48 hours. Virtually superimposable dose-response curves are obtained when scoring mutagenesis, induction of a phage lambda lysogen, or cell division delay (*4*). Many such curves were obtained with the maximum effect always between 1.5 and 2.5 m*M* H_2O_2. In this and subsequent figures, the results are those from a single experiment, representative of a minimum of three such experiments.

Department of Biochemistry, University of California, Berkeley, CA 94720.

*Present address: Department of Biochemistry, Duke University Medical Center, Durham, NC 27710.
†To whom correspondence should be addressed.